Polymer Chemistry

Photopatterning of Two Stage Reactive Polymer Networks with CO2-Philic Thiol-Acrylate Chemistry: Enhanced Mechanical Toughness and CO2/N2 Selectivity

Journal:	*Polymer Chemistry*
Manuscript ID	PY-ART-02-2022-000148.R1
Article Type:	Paper
Date Submitted by the Author:	04-Apr-2022
Complete List of Authors:	Blevins, Adrienne; University of Colorado Boulder Wang, Mengyuan; Oak Ridge National Laboratory, Chemical Science Division Lehmann, Michelle; Oak Ridge National Laboratory, Material Science and Technology Division Hu, Leiqing; University at Buffalo, Department of Chemical and Biological Engineering Fan, Shouhong; University of Colorado, Department of Mechanical Engineering Stafford, Christopher; National Institute of Standards and Technology, Polymers Division Killgore, Jason; National Institute of Standards and Technology, Lin, Haiqing; State University of New York at Buffalo, Chemical and Biological Engineering Saito, Tomonori; Oak Ridge National Laboratory, Chemical Sciences Division Ding, Yifu; University of Colorado, Mechanical Engineering

Photopatterning of Two Stage Reactive Polymer Networks with CO_2-Philic Thiol-Acrylate Chemistry: Enhanced Mechanical Toughness and CO_2/N_2 Selectivity

Adrienne K. Blevins[1], Mengyuan Wang[2], Michelle L. Lehmann[2,3], Leiqing Hu[4], Shouhong Fan[5], Christopher M. Stafford[6], Jason P. Killgore[7], Haiqing Lin[4], Tomonori Saito[2], Yifu Ding[1,5]

[1] Materials Science & Engineering Program, University of Colorado, Boulder, CO, 80303

[2] Chemical Sciences Division, Oak Ridge National Laboratory, Oak Ridge, Tennessee 37831

[3] The Bredesen Center for Interdisciplinary Research and Graduate Education, University of Tennessee, Knoxville, Tennessee 37996

[4] Department of Chemical and Biological Engineering, University at Buffalo, The State University of New York, Buffalo, NY, 14260

[5] Membrane Science, Engineering and Technology Center, Paul M. Rady Department of Mechanical Engineering, University of Colorado, Boulder, CO, 80309

[6] Materials Science and Engineering Division, National Institute of Standards and Technology, Gaithersburg, MD, 20899

[7] Applied Chemicals and Materials Division, National Institute of Standards and Technology, Boulder, CO, 80305

Abstract

Two Stage Reactive Polymer (TSRP) networks can be programmed with spatially varying heterogeneity, presenting a new way of designing material structure and controlling or enhancing properties. The formulation framework is versatile and can be applied to many different monomers to achieve desired performance. Such versatility is demonstrated here by designing a novel TSRP formulation that includes poly(ethylene oxide) (PEO) and polydimethylsiloxane (PDMS) groups to enhance gas permeability compared to previous thiol-acrylate TSRP formulations where permeability of certain gasses was too low to accurately measure. With this higher permeability, the effects of patterned heterogeneity on CO_2/N_2 selectivity were studied. A TSRP with 24 % to 34 % by weight PEO and PDMS groups, patterned with 50 μm circles of lower crosslinking density, is found to outperform the rule of mixtures prediction between permeability and selectivity for unpatterned materials. Comparing patterned films to Stage 2 films shows an increase in permeability by up to 98 % and an increase in selectivity by up to 67 %. Patterned films also show improved mechanical toughness (up to 46 % improvement) that previously studied TSRPs have. The material system presented in this study demonstrates a highly customizable approach for simultaneously improving permselective performance along with mechanical properties.

Introduction

CO_2 and N_2 separations are critical for many processes, including separating CO_2 from major emission sources such as flue gas, or natural gas.[1] Membranes are an attractive method of achieving high separation efficiency because they are energy-efficient, cost-effective, and have a smaller operational footprint. Polymeric membranes in particular are attractive because of their processability; however performance is hampered by a tradeoff between permeability and selectivity.[2,3] Many researchers have tried to combine different polymeric components in attempts to outperform the tradeoff: combining high permeability of one polymer with high CO_2 selectivity of another. One such pairing is poly(ethylene oxide) (PEO) and polydimethylsiloxane (PDMS). PEO is known for having a high affinity to CO_2 because of the polar ether groups in the chain but its permeability is limited.[4,5] PDMS, on the other hand, exhibits very high permeability due to the Si-O linkages that provide high mobility. Unfortunately, this high permeability accompanies low selectivity between gases.[6–8] Combinations of PDMS and PEO have been investigated in many ways, including copolymers, blends, and layering. Permselective performance is often improved, however fabrication can be difficult with complicated procedures, high prevalence of defects, or issues with compatibility of PEO and PDMS groups.[9–15]

Another effective way to combine different chemical groups within a material is to use a molecular architecture-based approach wherein carefully chosen monomers are polymerized to create a crosslinked material that includes specific functionalities. The thiol-ene reaction framework is an excellent example of this type of materials fabrication strategy because of the ease of use, controllable reaction rate, and readily achieved specific conversion with virtually limitless thiol and alkene monomer combinations.[16] Thiol-ene networks have successfully

incorporated PEO and PDMS chemistries for gas separations applications.[17,18] Hong et. al. achieved high CO_2/N_2 separation performance using thiol-PDMS monomers reacted with acrylate monomers. Some acrylates served as crosslinkers, and others added specific functionality. By tuning the formulations, CO_2 separation performance reached the upper bound values for high permeability and CO_2/N_2 selectivity established by Robeson in 2008.[19]

Recently, we demonstrated that a thiol-acrylate formulation can be harnessed to create two-stage reactive polymers (TSRPs). These are materials where the first stage is a lightly crosslinked network ("Stage 1") containing unreacted functional groups (C=C), that can subsequently react in a second curing step to make a more densely crosslinked material ("Stage 2").[20] The second curing step is designed to be light-initiated, and as a result can be spatiotemporally controlled. This leads to TSRPs with spatially controlled regions of Stage 1 (soft and more permeable) and Stage 2 (stiff and less permeable) material, all within a continuous network with tough interfaces.[21] Unlike the composite or layering fabrication strategies, TSRP fabrication allows for creation of films with precisely controlled spatial heterogeneity, which is only limited by the optical system used for second stage curing. Such precise spatial control can potentially be harnessed to engineer 3D patterned meta-membrane behavior with unprecedented selectivity.[22] Using one photopatterned TSRP system, we demonstrated that patterning in TSRPs can lead to mechanical and gas transport behavior that exceeds what would be expected of a rule-of-mixtures average of Stage 1 and Stage 2 properties.[21,23] However, CO_2 permeability of the TSRP formulation is very low (< 5 Barrer, where 1 Barrer = 3.35×10^{-16} mol $m^{-1}s^{-1}Pa^{-1}$) and no other light gas permeability was able to be measured accurately, leaving the effect of photopatterning on gas selectivity unexplored.

In this study, a novel thiol-acrylate TSRP network is developed that incorporates PEO and PDMS moieties to achieve higher gas permeability, based on modifications of the system reported by Hong et. al.[19] Photoinitiated two-stage behavior is demonstrated with a 20× increase in modulus and 50 °C increase in glass transition temperature (T_g) from Stage 1 to Stage 2. Multiple formulations with varying ratios of PEO and PDMS are studied. Films of the TSRP are photopatterned, and the effects of photopatterning on CO_2 permeability and CO_2/N_2 selectivity, as well as mechanical properties, are systematically investigated.

Experimental

Materials. (Mercaptopropyl) methylsiloxane homopolymer (1700-1800 g/mol) (Thiol-PDMS) and acyloxy terminated ethyleneoxide dimethylsiloxane-ethyleneoxide ABA block copolymer (1700-1800 g/mol) (EOPDMS) were purchased from Gelest Inc. Two types of poly(ethylene glycol) diacrylate (PEGDA) with molecular weight of 700 g/mol and 480 g/mol, pentaerythritol tetraacrylate (PETA), 2,2-dimethoxy-2-phenylacetophenone (DMPA), 2,6-di-tert-butyl-4-methylphenol (BHT), triethylamine (TEA) and inhibitor removers were purchased from Sigma-Aldrich. Dichloromethane (DCM) was purchased from Fisher Scientific. Both PEGDA 480 g/mol and PEGDA 700 g/mol had the inhibitors removed twice via filtering through a 20 ml syringe plugged with a small amount of cotton and inhibitor removers from bottom to top. Otherwise, all chemicals were used as received. DI water was obtained from a Millipore-Sigma Milli-Q system.

Film Fabrication. All films in Stage 1 were synthesized via the one-pot thiol-Michael addition reaction with base (TEA) as the catalyst. Taking a typical formula (PEGDA : EOPDMS molar ratio = 5.7:1) for example, 320 mg (5.80×10^{-5} mol) of Thiol-PDMS, 183 mg (1.04×10^{-4} mol) of EOPDMS, 414 mg (5.92×10^{-4} mol) of PEGDA, 286 mg (8.12×10^{-4} mol) of PETA (opened

and added in glove box), 36 mg (1 % of monomers in weight) of photo-initiator DMPA, 3.6 mg (0.1 % of monomers in weight) of acrylate free radical polymerization inhibitor BHT and 12.5 μl (1 % of monomers in weight) of base catalyst TEA were added into a 20 mL vial and dissolved in 5 mL DCM. The solution was shaken using a vortex mixer about 10 s and rested about 1 min until the solution became homogeneous and air bubbles dissipated. Then, the solution was poured into a leveled 8 cm diameter Teflon dish and covered by a piece of aluminum foil to block the visible light. During Stage 1 reaction, both the presence of oxygen, dark condition, and 0.1% in weight of added BHT aided in hindering photo-initiated free radical polymerization of the acrylate monomers. The Teflon dish was set in the fume hood overnight for thiol-Michael addition between Thiol-PDMS and EOPDMS, PEGDA and PETA to react completely and DCM to be fully evaporated. Finally, the free-standing Stage 1 film was gently detached from the Teflon dish. All Stage 1 films were between ≈90 μm and 160 μm in thickness.

Photopatterning. Stage 1 films were exposed to 365 nm UV light to initiate second stage curing. An OmniCure S2000 light with a mercury lamp and collimating adaptor was used for the exposure with 20 mW/cm^2 light intensity for 180 s. All films were laminated between glass (with or without an etched-chrome photomask) and a UV-absorbing neutral density filter (Thor Labs), according to previous experimental procedures.[21,23] The pattern etched into the chrome photomask consists of 50 μm diameter circles in a regular array, covering 50 % of the photomask area. The centers of circles are 62.7 μm apart from each other in both the vertical and horizontal directions. The curing parameters used here are based on previous work, allowing for full conversion to the second stage, while maintaining pattern resolution. Longer curing times can increase diffusion of radical species from the exposed pattern region, resulting in broad pattern interfaces.[24,25]

FTIR Measurements. A Nicolet 8700 FTIR spectrometer (Thermo Fisher Scientific, Waltham, MA) was used with the attenuated total reflection (ATR) accessory to analyze conversion of the first-stage reaction for all three formulations. ATR spectra were collected with 32 scans per spectrum at two different randomly chosen locations, and the data averaged.

Thermomechanical Measurements. A TA instruments (New Castle, DE) Q800 DMA was used to measure glass transition temperature (T_g), storage modulus, and tensile modulus of each formulation. Samples were cut into 4 mm x 12 mm rectangles. Tensile measurements were conducted at room temperature at a strain rate of 3 % per minute. Temperature sweeps were done from -140 °C to 100 °C at 3 °C/min under a strain amplitude of 0.125 % at 1 Hz. The value of T_g was taken to be the temperature at maximum internal loss (tan δ), and the rubbery plateau modulus was taken to be the storage modulus value at 90 °C.

Gas Permeation Testing. Permeability of the films was measured using a constant volume, variable pressure system. The testing apparatus was modeled after Singh, et al.[26] Film samples were sealed onto aluminum discs using epoxy resin, with 6.35 mm diameter active area for permeation testing. Samples were first placed under vacuum for at least 8 hours to remove any residual solvent and absorbed gasses, followed by a leak rate measurement, which was subtracted from the permeation measurements. After the leak rate measurement, 103 kPa (15 psi) of the permeation gas was applied, and permeation through the film was measured for 3 hours to 8 hours. The permeation test was repeated twice more, with vacuum being drawn between each repeat measurement. N_2 was always tested before CO_2 to avoid any potential plasticization effect from CO_2.

Solubility Testing. A gravimetric sorption analyzer (Hiden Isochema IGA 001, Warrington, UK) was used to determine CO_2 sorption of the samples at 35 °C and varied pressures from 1 bar

to 3 bar.[27] Around 70 mg of the sample was loaded and dried under vacuum at 35 °C until the sample weight was stable. The density of the sample film was calculated based on the corresponding mass and volume. Gas solubility was calculated from the weight change of the sample with the consideration of the buoyancy effect at each pressure. The uncertainty of the gas solubility was estimated at ≈10 % using an error propagation method.[27] N_2 solubility was too low to accurately measure.

Atomic Force Microscopy (AFM). An Asylum Research Cypher AFM (Santa Barbara, CA) instrument was used in Fast Force Mapping mode to measure surface modulus of photopatterned films. A force modulation mode tip (FMR, Nanosensors, Switzerland) was used with a force setpoint of ≈80 nN. The Hertz contact model was used to estimate modulus values from the force-distance data. Both cross sections and surfaces of the samples were measured to characterize the 3D profiles of the patterned Stage 1 and 2 films. Flat and smooth cross sections of the samples were created by cryomicrotoming (Leica, EM FC7, Buffalo Grove, IL) with a diamond blade at -120 °C.

Water Contact Angle (WCA). The surface wettability of sample films was characterized using water contact angle measurements at room temperature. A sessile-drop method (2 μL DI-water droplet) was used with an optical tensiometer (Attension Theta Lite, Biolin Scientific). For each sample, at least three repeated measurements were carried out, and the average values are reported here.

X-ray Photoelectron Spectroscopy (XPS). XPS measurements were performed on a Kratos AXIS Ultra DLD Spectrometer (Kratos Analytical, Manchester, UK) using a monochromatic Al K_α source (1486.6 eV) operated at 140 W. The base pressure of the sample analysis chamber was ≈ 1.33×10^{-7} Pa (1×10^{-9} Torr), and spectra were collected from a nominal spot size of 300 μm ×

700 μm. Measurements were performed in hybrid mode using electrostatic and magnetic lenses. For the survey scans presented here, the pass energy of the analyzer was set at 160 eV with an energy resolution 0.5 eV and dwell time of 0.1 s. Atomic composition was determined from the survey scans using the CasaXPS software package.

Results and Discussion

Single stage characterization

In our prior work, thiol (pentaerythritol tetrakis(3-mercaptopropionate), or PETMP) – acrylate (trimethylolpropane triacrylate, or TMPTA) TSRPs that have a significant difference in T_g between Stage 1 (T_g = -10 ℃) and Stage 2 (T_g = 43 ℃) were formulated with a 2:1 acrylate:thiol functional group ratio.[20,21,23] The base-catalyzed thiol-Michael addition reaction polymerizes the multifunctional monomers into a lightly crosslinked material (Stage 1). All thiol groups react with acrylate groups, and an excess of unreacted acrylates remain, tethered to the network, which is further crosslinked upon photo-initiated free-radical polymerization into a highly crosslinked material (Stage 2). The PETMP-TMPTA based thiol-acrylate TSRP system exhibited low CO_2 permeability: (4.37 ± 0.57) Barrer and (0.37 ± 0.18) Barrer (1 Barrer = 3.35×10^{-16} mol $m^{-1}s^{-1}Pa^{-1}$) for Stage 1 and Stage 2 films, respectively.[23]

In a recent work by Hong et. al., a PDMS monomer with 40 pendant thiols was used alongside a mono-functional (poly(ethylene glycol) methyl ether acrylate, PEGMEA) and difunctional acrylate (EOPDMS) in the best performing formulations.[19] CO_2 permeability of the two formulations that landed on the Robeson upper bound were (930 ± 30) Barrer and (820 ± 20) Barrer with CO_2/N_2 selectivity of 37.5 ± 0.9 and 39.0 ± 1.2, respectively. This was the basis for the new TSRP formulation in this work, with additional acrylate groups incorporated to obtain

the (thiol : acrylate) functional group ratios necessary for achieving distinct, two-stage behavior. To keep the PDMS and PEO content high, EOPDMS remained in the formulation, while PEGMEA was replaced with PEGDA. When only difunctional acrylates PEGDA and EOPDMS were used, the formulation did not form stable Stage 1 films because the percolation threshold for network formation was not reached. To remedy this, a tetra-functional acrylate monomer, PETA was incorporated to improve structural stability through added network connectivity. All monomer structures are shown in Figure 1A.

TSRP films with three different formulations were made, all with constant amounts of thiol-PDMS and PETA. PETA was present in a 14:1 molar ratio to thiol-PDMS. The total amount of PEGDA and EOPDMS in the formulations was also constant, but the molar ratio of PEGDA : EOPDMS (how the different formulations are referred to throughout the paper) was varied. All formulation details are listed in Table 1.

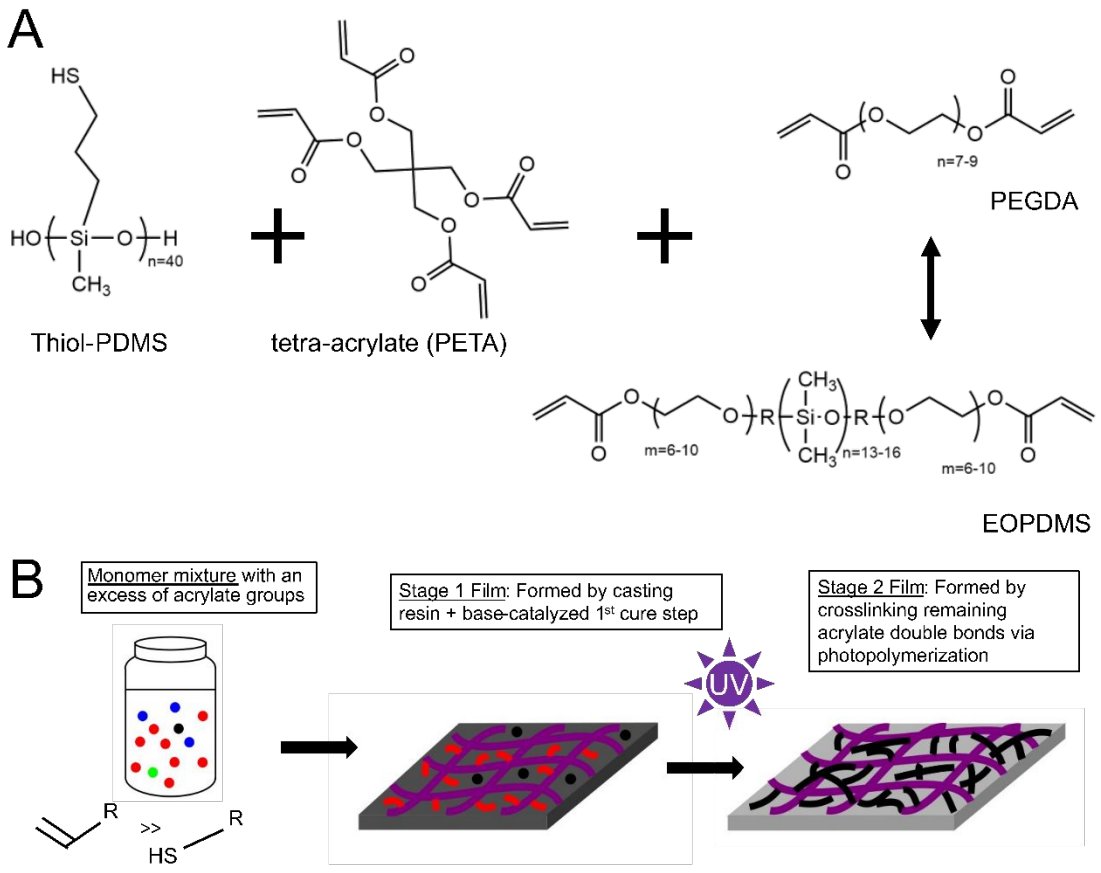

Figure 1. (A) Monomers used to synthesize the PDMS/PEO-containing TSRP films. The three different formulations investigated in this study use different ratios of PEGDA : EOPDMS (Table 1). (B) A schematic showing how films are made from the monomers.

Table 1. Monomer ratios and mass percent of PDMS and PEO groups for all three formulations investigated in this study. All molar or functional group ratios are relative to 1 mole of thiol-PDMS or 1 mole thiol functional group, respectively.

	Wt. % Active Groups		**Monomer Molar Ratios**		
Formulation Name	PEO	PDMS	PEGDA : EOPDMS	PEGDA : Thiol-PDMS	EOPDMS : Thiol-PDMS
1.4:1	27	34	1.4	7	5
3:1	29	28	3	9	3

5.7:1	31	24	5.7	10.2	1.8

All samples reached a 2:1 acrylate : thiol functional group ratio, and the weight percentages of PDMS and PEO groups range from 24 % to 34 %. Another point to note is that by varying amounts of EOPDMS and PEGDA, the average molecular weight between crosslinks, M_c, is also altered. EOPDMS has a much higher molecular weight than PEGDA, as shown in Figure 1A, so formulations with higher amounts of EOPDMS will have a higher average M_c, and vice-versa. A schematic is provided in Figure 1B to illustrate how films are made. Monomers are mixed together with catalyst and photoinitiator and react under ambient conditions to form Stage 1 films. Those Stage 1 films can then be exposed to UV light to further crosslink acrylate functional groups, forming Stage 2 films.

The completeness of the Stage 1 thiol-Michael reaction was investigated by measuring thiol conversion via FTIR.[28] Figure 2A shows the spectra for each formulation after the thiol-Michael addition. The S-H stretching vibration peak at 2560 cm^{-1} is not present in any sample, indicating complete reaction of thiol groups. In addition, the C=C stretching vibration peak is still present at 1638 cm^{-1}, indicating that there are unreacted acrylates remaining in the Stage 1 network to participate in the UV-initiated Stage 2 reaction.

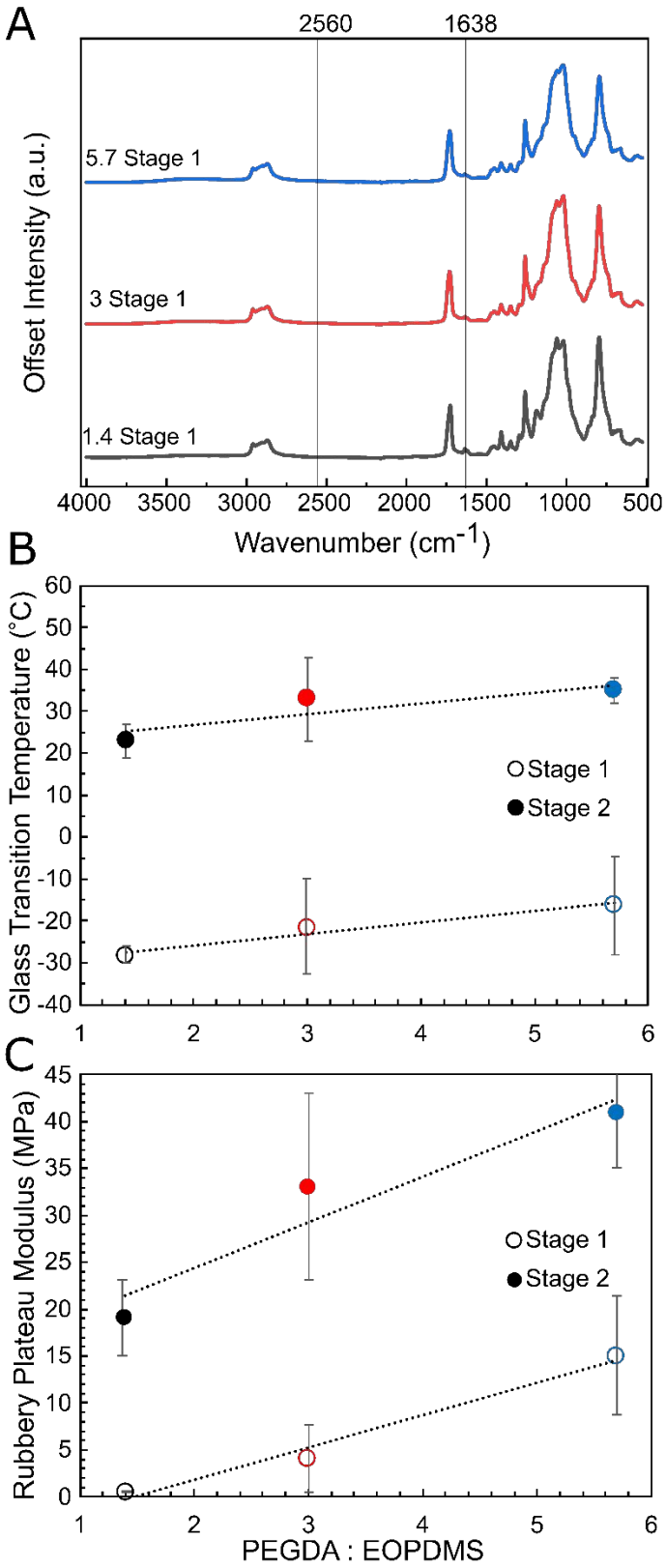
A
2560
1638
5.7 Stage 1
3 Stage 1
1.4 Stage 1
Offset Intensity (a.u.)
4000 3500 3000 2500 2000 1500 1000 500
Wavenumber (cm-1)
B
Glass Transition Temperature (°C)
60 50 40 30 20 10 0 -10 -20 -30 -40
1 2 3 4 5 6
Stage 1
Stage 2
C
Rubbery Plateau Modulus (MPa)
45 40 35 30 25 20 15 10 5 0
1 2 3 4 5 6
PEGDA : EOPDMS
Stage 1
Stage 2

Figure 2. (A) FTIR spectra of films for each formulation after Stage 1 thiol-Michael addition reaction. 2560 cm^{-1} is the -SH stretching peak and 1638 cm^{-1} is the C=C stretching peak.[19] (B) and (C) show the T_g and rubbery modulus (determined at 90 ºC by DMA) evolution from Stage 1 (empty symbols) to Stage 2 (filled symbols) for each of the three formulations, correspondingly. (B) and (C) share the same x-axis, the molar ratio of PEGDA : EOPDMS, relative to one mole of EOPDMS. Dashed lines in (B) and (C) are included to guide the eye for overall trend between formulations. Colors in the figure represent the formula: black corresponds to the 1.4:1 formulation, red to 3:1, and blue to 5.7:1.

Figures 2B and 2C show the T_g and rubbery plateau modulus (E'_R, measured at 90 °C and 1 Hz frequency loading) for both Stage 1 and Stage 2 films for each formulation. For Stage 1 films, both T_g and E'_R increase with the PEGDA : EOPDMS ratio, which is consistent with the increase of crosslinking density (or reduced M_c, as $M_c \sim 1/E'_R$) as mentioned above. Upon second stage curing, each formulation showed an increase in both T_g (by 50 °C to 55 °C) and E'_R (by 20 MPa to 30 MPa). Between the formulations, there was an overall increase in T_g and E'_R with increased PEGDA ratios for the Stage 2 films obtained. Regardless, two-stage network behavior is confirmed for all three formulations, with a large increase in thermomechanical properties from Stage 1 to Stage 2.

Patterning of the TSRP films

Films for each formulation were photo-patterned to obtain 50 μm diameter Stage 1 circles within a Stage 2 matrix. In our previous work of PETMP-TMPTA formulated TSRP films, a decrease in CO_2 permeability was observed when Stage 2 continuous phase was patterned with 10 μm Stage 1 circles.[23] Small misalignments within the photopatterning equipment setup can

lead to poor pattern replication at such length scales, however, so a larger pattern size was chosen for this work to minimize pattern fidelity issues. It is hypothesized, however, that patterns with higher amounts of interfacial length (smaller patterns, higher areal density, etc.) slow gas diffusion in patterned membranes; work on this topic is ongoing. Figure 3A presents a schematic of the photopatterning process. 50 µm patterns were hypothesized to be small enough to still show a structure-induced effect. A representative optical image of this pattern in a film of the 3:1 formulation is shown in Figure 3B. Faithful replication of the circle shape is observed, and the average diameter of the Stage 1 circles is (46.7 ± 1.3) µm.

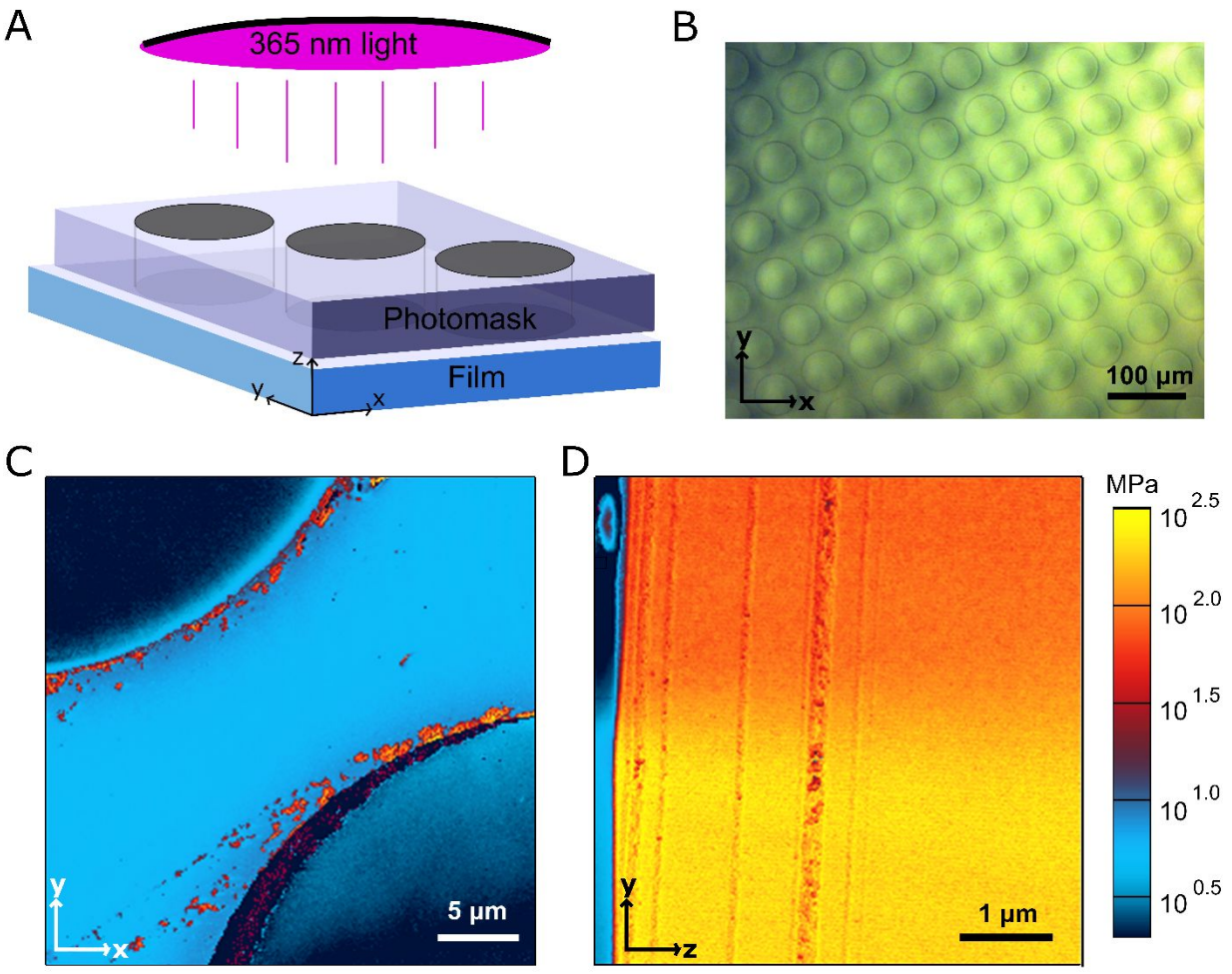

Figure 3. Photopattern replication in TSRP films; formulation 3:1 was chosen as the representative system, as all formulations exhibited this behavior. (A) Schematic of the photopatterning process with coordinate system defined. (B) Optical microscope image of 50 μm circles patterned into the top surface of the films. (C) AFM-generated modulus map of the film surface capturing Stage 1 circles in Stage 2 matrix. (D) AFM-generated modulus map of the cross-section surface showing the interface between Stage 1 and Stage 2 regions through the film thickness, as well as the thin layer of low modulus material on the far left. Coordinate axis are provided in (B) – (D) to help orient the plane on which the image was taken. (C) and (D) share the same color scale.

AFM modulus mapping at both the surface (Figure 3C) and a cross-section through the thickness (Figure 3D) were carried out to assess the fidelity of pattern transfer and to accurately quantify the volume fraction of Stage 1 and 2. In the surface modulus map, Figure 3C, modulus values within the circles are (2.3 ± 0.3) MPa and values in the matrix are (5.5 ± 0.3) MPa. Both average values are consistent with what is expected of Stage 1, based on pure Stage 1 scans (Figures S1-3, Table S1). Surprisingly, modulus values of the Stage 2 matrix are much lower than that of the pure Stage 2 measurements (Figures S1-3, Table S1), which have values ranging from 100 MPa to 150 MPa. Despite excellent pattern replication, there is not much modulus contrast in the photopatterned surface. The modulus contrast that is present between circles and matrix comes from height differences between the two regions due to shrinkage and photomask imprinting occurring with UV exposure (Figure S4) as well as differences in the modulus values beneath the surface. The cross-sectional modulus map (taken at the top edge of the patterned film, Figure 3D) shows higher modulus values underneath the surface, along with a clear interface between the Stage 1 and 2 regions. The modulus value of Stage 2 region is on average

(161 ± 37) MPa, which matches up much better with that of pure Stage 2 measurements. However, Stage 1 region is on average (67 ± 11) MPa, indicating some partial curing. This partial curing effect is accounted for in calculations of rule-of-mixtures permeability estimates, as detailed in the SI. An important note is that these AFM-generated modulus values are much higher than values for the rubbery plateau modulus (Figure 2C) because AFM measurements are carried out at higher frequency (200 Hz vs. 1 Hz) and lower temperature (room temperature vs. 90 °C).

The discrepancy between surface and cross-sectional modulus values is due to a soft layer present at the top of the sample (the film surface pressed against the photomask), which can be seen as the blue strip in Figure 3D. Larger, full view cross-sectional scans of both top and bottom surfaces are presented in Figure S5. The modulus values for this approximately 250 nm thick layer align well with the surface values in Figure 3C. This soft layer could be a result of PDMS enrichment, as PDMS-containing sections of the network may preferentially orient toward free surfaces to reduce surface energy. This also occurs in the well-studied phenomenon of hydrophobic recovery, which affects many other applications that utilize PDMS materials.[29] Studies have also shown that UV-curing and second-stage curing can induce phase separation due to the increase in crosslinking density, which may also be contributing to PDMS enrichment upon photopatterning.[10,30–32] Water contact angle measurements (Figure S6) and XPS (Table S2) were performed on the top surface of Stage 1 and 2 films to identify any evidence of higher PDMS content. Water contact angle showed a 22.8º increase from Stage 1 (67.7º ± 1.4º) to Stage 2 (90.5º ± 3.5º) surface, showing an increase in hydrophobicity. XPS was also measured for confirmation of increased Si presence, and results showed an increase in Si atomic percentage from (11.34 ± 0.19) at.% to (14.78 ± 0.36) at.%. This lends evidence to a soft, PDMS-rich region

at the surface. With a higher PDMS content at the surface, the layer will have higher local permeability, allowing ambient oxygen to diffuse faster through the layer during the photopatterning process. This could lead to oxygen inhibition reducing curing within the layer as well. Finally, the soft layer could also be contributing to the partial curing of Stage 1 regions within the rest of the sample, as it provides another interface that can scatter light. However, the presence of this soft, PDMS-rich surface layer is not expected to significantly alter permeability or mechanical results because it only amounts to 0.2 vol.% of a 150 μm thick sample and will not provide much resistance to gas molecules given the high permeability of PDMS. A sample calculation in the Supplementary Information (Section S3) shows that not including the soft, highly permeable layer changes the predicted gas permeability values by 0.1 % to 0.5 %.

Bulk Mechanical Properties

In our previous studies with PETMP-TMPTA TSRPs, patterning films improved bulk mechanical properties, primarily tensile toughness.[21,23] Here, we conducted similar mechanical analysis to determine if these new formulations also behave in such a manner. The results of tensile tests are shown in Figure 4, plotting tensile toughness (estimated using area under the stress-strain curves) against tensile modulus. Stage 1, on average, has a low modulus between 2 and 3 MPa, depending on formulation, while Stage 2, expectedly, has a higher modulus at 40 - 60 MPa. The Stage 1 tensile modulus values are on order with the rubbery plateau moduli values, as tensile tests were taken at room temperature, when these films were in the rubbery state. Stage 2 tensile modulus values, however, are higher than rubbery plateau modulus values (Figure 2C) due to the films being in a glassy or transitionary state at the tensile measurement temperature. Also, all values are less than AFM-measured modulus values (Figures S1-S3) due to the low strain rate measured here as opposed to the high frequency AFM measurement. The moduli of

the patterned samples lie between both Stage 1 and Stage 2 values, in between a Voigt and Reuss model rule-of-mixtures calculation. This is consistent with literature on uniformly distributed soft inclusions in a stiff matrix.[33] All unpatterned samples have tensile toughness values ranging between 90 kJ/m^3 and 140 kJ/m^3 with Stage 2 samples showing slightly lower toughness. Upon patterning 50 µm Stage 1 circles in a Stage 2 matrix, the toughness increases 40 % to 45 % from a 50/50 volumetric average of Stage 1 and 2 toughness values for the three formulations. Even more significantly, the toughness values are consistently larger than pure Stages 1 and 2 as well, across all formulations. This absolute enhancement is attributed to an increased strain-to-failure associated with the interfaces between Stage 1 and 2, which can act as a barrier for crack propagation as previously reported in Kolednik et. al.[34]

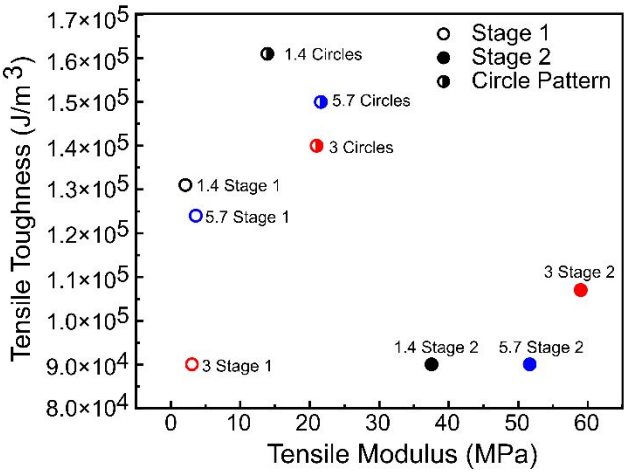

Figure 4. Tensile toughness vs. tensile modulus for Stage 1, Stage 2, and 50 µm Stage 1 circles with all 3 formulations. Colors in the figure represent the formula: black corresponds to the 1.4:1 formulation, red to 3:1, and blue to 5.7:1.

Gas Transport Properties

Solubility testing was conducted for Stage 1 and Stage 2 samples for each formulation, and the sorption coefficients for CO_2 are shown in Figure 5A. Overall, the values (ranging from (1.2 to 1.0) cm^3(STP)/cm^3atm) sit between what was previously seen in thiol-acrylate TSRPs ((0.9 to 1) cm^3(STP)/cm^3atm) and pure crosslinked PDMS and PEO ((1.3 to 1.4) cm^3(STP)/cm^3atm).[6,35] This confirms that the PDMS and PEO functional groups added into a thiol-acrylate TSRP did improve CO_2 sorption. The working range of solubility is quite small with crosslinked networks, however, and most permeability improvements in these formulations will be a result of increases in diffusivity. Between Stage 1 and Stage 2 for each formulation there is a decrease in solubility that follows the trend of increase in crosslinking density and decrease in free volume.[36,37] Between formulations, there is also a trend of decreasing solubility with increasing crosslinking density (or decreasing free volume), mirroring the trends seen in thermomechanical properties between all three formulations. This outweighs any subtle effect from functional group contribution between PEO and PDMS. Since the solubility of CO_2 in PEO is higher than PDMS, one would expect the trend to increase with increasing PEO content (with 5.7:1 being the highest). But the opposite trend is observed, indicating free volume to be the dominant parameter within the formulation space explored here. When looking at the wt.% values in Table 1 for PEG and PDMS groups, they only span a difference of about 10 %, which is relatively small. Investigating the effect of larger changes in functional group percentages on solubility within a TSRP would be worthwhile for the future. Also, due to low values, N_2 solubility cannot be accurately determined, but is assumed to follow the same trends as CO_2. Patterned samples were not tested as previous work indicated solubility simply falling between Stage 1 and Stage 2 values, which are not significantly different to begin with.

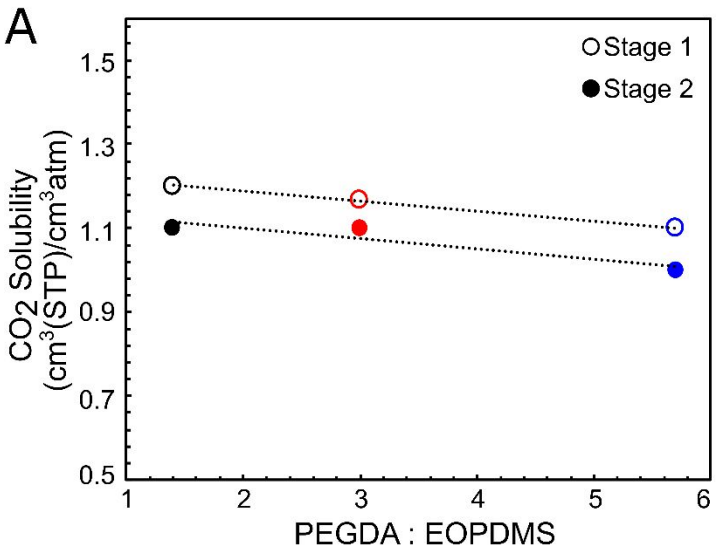
A
Stage 1
Stage 2
CO_2 Solubility (cm^3(STP)/cm^3atm)
1.5
1.3
1.1
0.9
0.7
0.5
1
2
3
4
5
6
PEGDA : EOPDMS

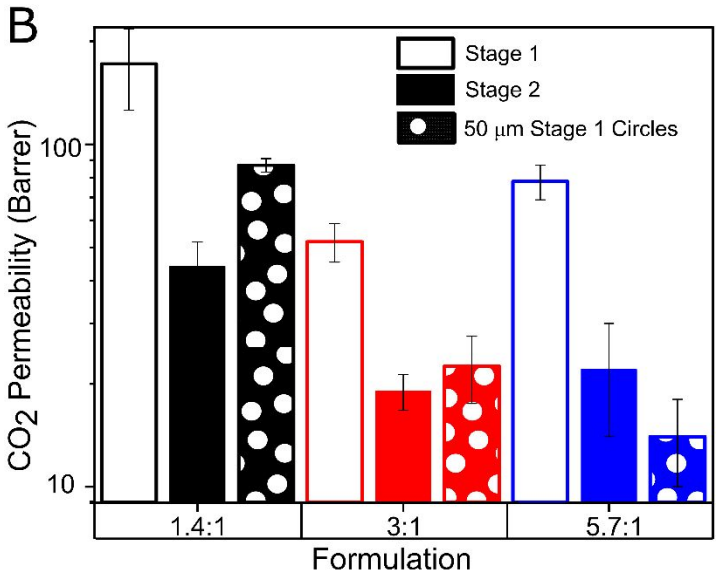
B
Stage 1
Stage 2
50 μm Stage 1 Circles
CO_2 Permeability (Barrer)
100
10
1.4:1
3:1
5.7:1
Formulation

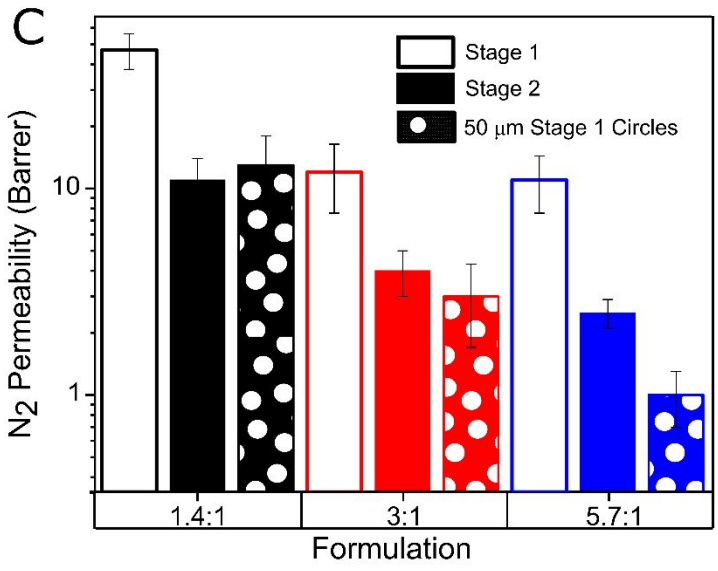
C
Stage 1
Stage 2
50 μm Stage 1 Circles
N_2 Permeability (Barrer)
10
1
1.4:1
3:1
5.7:1
Formulation

Figure 5. (A) CO_2 solubility for Stage 1 and 2 samples of each formulation. Dashed lines included to guide the eye for the overall trend between formulations. Empty symbols represent Stage 1 samples and filled symbols represent Stage 2. (B) and (C) show the CO_2 and N_2 permeability for all samples, correspondingly. 1 Barrer = 3.35×10^{-16} mol $m^{-1}s^{-1}Pa^{-1}$. Colors in the figure represent the formula: black corresponds to the 1.4:1 formulation, red to 3:1, and blue to 5.7:1.

Permeability of both CO_2 and N_2 was measured for all samples, as shown in Figures 5B and C, correspondingly. Comparing again to previous thiol-acrylate TSRPs, the CO_2 permeability is more than one-order of magnitude higher for the unpatterned Stage 1 and Stage 2 films.[23] Moreover, N_2 permeability was successfully measured with an error similar to the CO_2 measurements. This indicates that the PEO and PDMS groups within the network are assisting to improve permeability for both gases. Permeability values for the TSRP samples here, however, are more than one-order of magnitude less than those in the study conducted by Hong et. al.[19] This is attributed to the addition of tetraacrylate (PETA), which was necessary to yield a stable Stage 1 film. Compared to literature, the permeabilities of the TSRP films presented here are similar to those in Kwisnek et. al., where thiol-ene networks that incorporated 35 % to 65 % by weight PEG groups had CO_2 permeability values ranged from 25 Barrer to 90 Barrer, and N_2 permeability values from 0.5 Barrer to 2 Barrer.[17] Permeability of both CO_2 and N_2 decreases with increase of PEGDA : EOPDMS ratio for Stage 1 films. For all three formulations, Stage 2 curing significantly reduced the permeability of both gases. Specifically, all formulations show about a 3-4 times reduction in CO_2 and N_2 permeability.

Interestingly, measured permeability of the patterned TSRP films is lower than a rule of mixtures prediction using values of the pure Stage 1 and 2 samples. At an initial glance, the

permeabilities of the patterned TSRPS films for both CO_2 and N_2 lie very close to Stage 2 values, or below them. To fully quantify this, a volume-fraction weighted average (considering partial curing and pattern interfacial width, as detailed in the SI) is calculated between Stage 1 and Stage 2 for each formulation. The patterned sample permeabilities are then calculated as a percentage decrease from said calculated spatial average. This is shown in Figure 6A, where the spatial average for each formulation is set to 0 on the y-axis (values are found in Table S3). On average, CO_2 permeability is 23 % less and N_2 permeability is 49 % less than predicted. The 5.7:1 formulation has the largest percent decrease for both gasses, while 1.4:1 has the smallest percent change. Evidently, a larger degree of permeability reduction is observed for formulations with higher T_g value for Stage 2 film. The difference in percentages for CO_2 and N_2 indicates that the effect of the patterning on the gas permeability depends on the gas type. The N_2 percentage decreases are similar to those previously seen for CO_2 in our previous thiol-acrylate TSRP research.[23] This indicates that the structure-induced permeation decrease is less pronounced for CO_2, likely because of the CO_2-philic groups. Such gas-specific pattern-induced permeability reduction influences the selectivity values, which are plotted in Figure 6B.

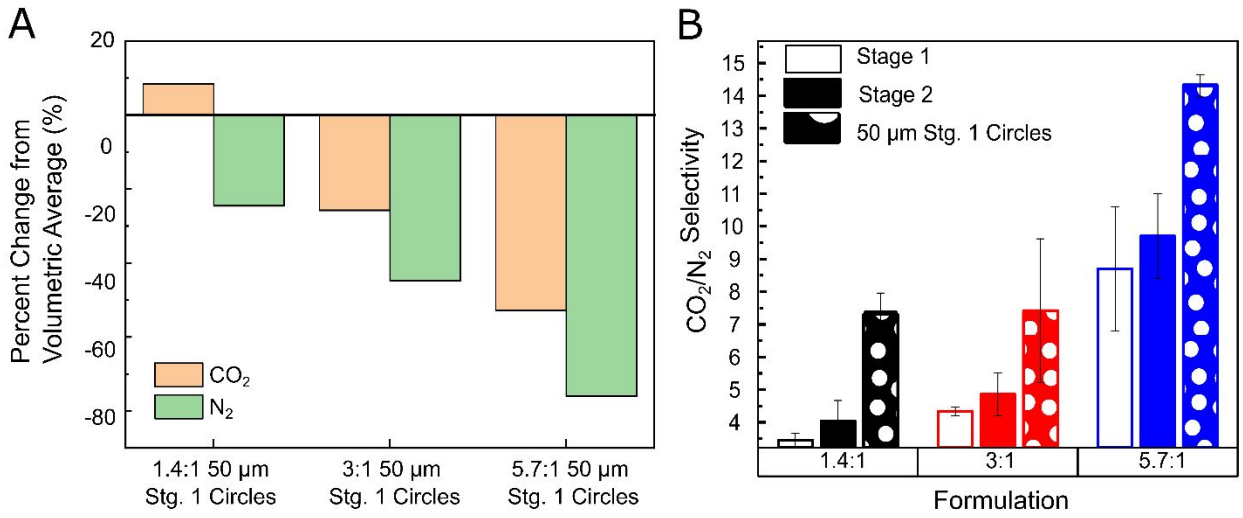

Figure 6. (A) Compares measured photopatterned sample average permeability as a percent decrease from the anticipated area fraction-averaged permeability of Stage 1 and 2 values for each formulation and test gas. (B) CO_2/N_2 selectivity for all samples.

From Stage 1 to Stage 2, the CO_2/N_2 selectivity increases, which follows typical selectivity versus permeability tradeoff: the formulations with larger permeability reduction from Stage 1 to Stage 2 conversion show a larger increase in selectivity. The difference in selectivity between Stage 1 and 2 of the 1.4:1 formulation is very small as the Stage 2 film has a T_g close to room temperature (Figure 2B). Pure Stage 1 and 2 selectivity values fall between pure PEO and PDMS values, as expected. Given the relatively small difference in solubility between Stage 1 and 2 for all three formulations (Figure 5A), the selectivity increase is mostly contributed by the diffusivity selectivity.[14] CO_2/N_2 permeability selectivity values are lower than other PEG-containing thiol-ene networks, however the diffusive selectivities are much higher.[17] For each of the three formulations, the patterned films showed the highest CO_2/N_2 selectivity. For the 1.4:1 and 5.7:1 formulations, the patterned film CO_2/N_2 selectivity is statistically significantly higher than the Stage 2 film at a confidence interval of 90 % using a one-sided t-test. Because the N_2 permeability decreases from the patterning much more than the CO_2 permeability, and the solubility values are assumed to effectively stay constant with patterning, it can be concluded that N_2 diffusivity decreases more than CO_2 diffusivity, which leads to an even larger increase in diffusivity selectivity. Patterning causes a structural effect that increases diffusivity selectivity even further than just a simple increase in crosslinking density. When plotted on a Robeson tradeoff plot (Figure 7), for formulations 1.4:1 and 3:1, the patterned sample moves in the direction of breaking the tradeoff that exists between CO_2 permeability and CO_2/N_2 selectivity for both Stage 1 and 2 of the material. Specifically, the 1.4:1 formulation shows that the

patterned sample has statistically significantly higher CO_2 permeability and CO_2/N_2 selectivity than Stage 2, again based on a 90 % confidence interval. This performance improvement is perpendicular to the property average line that can be drawn between Stages 1 and 2 for a specific formulation. Selectivity is increased beyond Stage 1 and 2 values for patterned films, but CO_2 permeability is not sacrificed to values below Stage 1 and 2, instead falling in between. For the 1.4:1 formulation, the permeability is still significantly larger than Stage 2. The combination of high toughness and high CO_2 permeability for the 1.4:1 circles sample is highly optimized. Controlling the photopatterned structure of the TSRP films improves both tensile toughness and CO_2/N_2 selectivity in the direction of common tradeoffs. It has been consistently shown in our previous work that photopatterned TSRPs, with micron-scale patterns, outperform tradeoffs that exist with unpatterned counterparts, and this novel TSRP formulation that includes PEO and PDMS groups is no different.[21,23] This continues to show the effectiveness of the TSRP materials fabrication strategy at reaching performance goals through tunability, both with monomer chemistry and photopatterned structure. Future work will continue to look at optimizing permselective performance through photopatterning and will focus on the roles of pattern geometry, and modulus contrast between Stages 1 and 2.

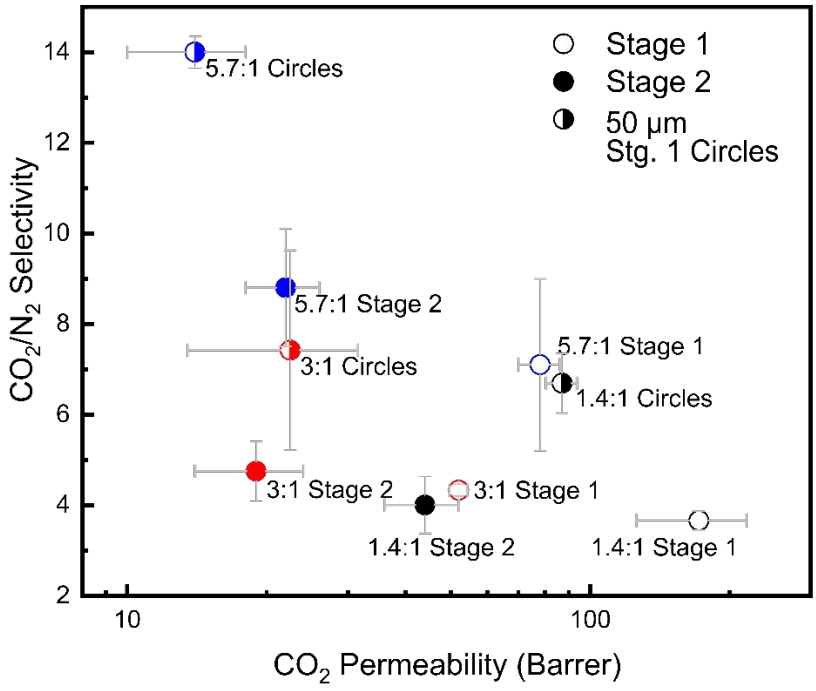

Figure 7. Robeson plot of average CO_2/N_2 selectivity versus average CO_2 permeability for all samples. 1 Barrer $=3.35\times10^{-16}$ mol $m^{-1}s^{-1}Pa^{-1}$. Colors in the figure represent the formula: black corresponds to the 1.4:1 formulation, red to 3:1, and blue to 5.7:1.

Conclusions

In this study, a novel thiol-acrylate based TSRP that includes PEO and PDMS groups at 24 % to 34 % by weight was successfully created. This is the first reported instance of a TSRP network with PEO and PDMS functionality; this was achieved by utilizing thiol and acrylate monomers that contain PEO and PDMS functional groups. A significant difference in thermomechanical properties was observed between Stage 1 and Stage 2 curing, and films of the TSRP were successfully patterned with 50 µm Stage 1 circles. All photopatterned materials exhibited enhanced tensile toughness from pure Stages 1 and 2, as well as reduced gas permeability from geometric averages of pure Stage 1 and 2 values. With the addition of PEO

and PDMS groups, however, overall permeability values were much higher than previously studied TSRP materials. Because of this, N_2 permeability, and therefore CO_2/N_2 selectivity, could be studied. Permselective performance of the three formulations was found to depend more on M_c and free volume than concentration of PDMS and PEO groups. Photopatterning was found to affect CO_2 permeability coefficients disproportionately to N_2 permeability, which led to an increase in CO_2/N_2 selectivity. When plotted on a tradeoff graph with CO_2 permeability, the patterned samples outperform a tradeoff created between Stage 1 (higher permeability, lower selectivity) and Stage 2 materials (lower permeability, higher selectivity). Photopatterning TSRPs is a facile materials fabrication strategy to create a polymer composite that outperforms rule of mixtures behavior for mechanical and permselective properties.

Author Contributions

Conceptualization: AB, ML, JK, TS, YD; Data curation: AB; Formal analysis: AB, JK; Funding acquisition: YD; Investigation: AB, MW, ML, LH, SF, CS; Methodology: AB, ML, MW, JK; Project administration: AB, YD; Resources: ML, MW, TS; Supervision: AB, YD, TS; Visualization: AB, Writing – original draft: AB, MW, LH, SF, CS; Writing – review and editing: AB, MW, ML, LH, CS, JK, HL, TS, YD.

Conflicts of Interest

There are no conflicts to declare.

Acknowledgements

The authors gratefully acknowledge research support from the National Science Foundation (NSF) Industry/University Cooperative Research Center for Membrane Science, Engineering and Technology (MAST) at the University of Colorado Boulder (UCB, award number, IIP 1624602).

Acknowledgement is made to the Donors of the American Chemical Society Petroleum Research Fund for partial support of this research. The Stage 1 film synthesis and design work is supported by the U.S. Department of Energy, Office of Science, Materials Sciences and Engineering Division. AB acknowledges the support from GAANN fellowship for Soft Matter and also thanks Tayler Hebner for the FTIR measurements, as well as Chamaal Karunaweera for access to data collection resources.

References

1 M. Chawla, H. Saulat, M. Masood Khan, M. Mahmood Khan, S. Rafiq, L. Cheng, T. Iqbal, M. I. Rasheed, M. Z. Farooq, M. Saeed, N. M. Ahmad, M. B. Khan Niazi, S. Saqib, F. Jamil, A. Mukhtar and N. Muhammad, *Chem. Eng. Technol.*, 2020, **43**, 184–199.
2 L. M. Robeson, *J. Membr. Sci.*, 2008, **320**, 390–400.
3 H. B. Park, J. Kamcev, L. M. Robeson, M. Elimelech and B. D. Freeman, *Science*, 2017, **356**, eaab0530.
4 H. Lin and B. D. Freeman, *J. Membr. Sci.*, 2004, **239**, 105–117.
5 S. L. Liu, L. Shao, M. L. Chua, C. H. Lau, H. Wang and S. Quan, *Prog. Polym. Sci.*, 2013, **38**, 1089–1120.
6 T. C. Merkel, V. I. Bondar, K. Nagai, B. D. Freeman and I. Pinnau, *J. Polym. Sci. Part B Polym. Phys.*, 2000, **38**, 415–434.
7 S. S. Madaeni, M. M. S. Badieh and V. Vatanpour, *Polym. Eng. Sci.*, 2013, **53**, 1878–1885.
8 L. M. Robeson, B. D. Freeman, D. R. Paul and B. W. Rowe, *J. Membr. Sci.*, 2009, **341**, 178–185.
9 S. R. Reijerkerk, M. H. Knoef, K. Nijmeijer and M. Wessling, *J. Membr. Sci.*, 2010, **352**, 126–135.
10 Y. Gu, S. Zhou, H. Luo, L. Wu, W. Gao and J. Yang, *J. Polym. Sci. Part B Polym. Phys.*, 2016, **54**, 1612–1623.
11 S. R. Reijerkerk, M. Wessling and K. Nijmeijer, *J. Membr. Sci.*, 2011, **378**, 479–484.
12 A. Halim, Q. Fu, Q. Yong, P. A. Gurr, S. E. Kentish and G. G. Qiao, *J. Mater. Chem. A*, 2014, **2**, 4999.
13 T. Hu, G. Dong, H. Li and V. Chen, *J. Membr. Sci.*, 2014, **468**, 107–117.
14 I. Hossain, D. Kim, A. Z. Al Munsur, J. M. Roh, H. B. Park and T.-H. Kim, *ACS Appl. Mater. Interfaces*, 2020, **12**, 27286–27299.
15 X. Ren, J. Ren, H. Li, S. Feng and M. Deng, *Int. J. Greenh. Gas Control*, 2012, **8**, 111–120.
16 C. E. Hoyle and C. N. Bowman, *Angew. Chem. Int. Ed.*, 2010, **49**, 1540–1573.
17 L. Kwisnek, J. Goetz, K. P. Meyers, S. R. Heinz, J. S. Wiggins and S. Nazarenko, *Macromolecules*, 2014, **47**, 3243–3253.
18 V. A. Kusuma, E. A. Roth, W. P. Clafshenkel, S. S. Klara, X. Zhou, S. R. Venna, E. Albenze, D. R. Luebke, M. S. Mauter, R. R. Koepsel, A. J. Russell, D. Hopkinson and H. B. Nulwala, *J. Polym. Sci. Part Polym. Chem.*, 2015, **53**, 1548–1557.

19 T. Hong, P.-F. Cao, S. Zhao, B. Li, C. Smith, M. Lehmann, A. J. Erwin, S. M. Mahurin, S. R. Venna, A. P. Sokolov and T. Saito, *Macromolecules*, 2019, **52**, 5819–5828.
20 D. P. Nair, N. B. Cramer, J. C. Gaipa, M. K. McBride, E. M. Matherly, R. R. McLeod, R. Shandas and C. N. Bowman, *Adv. Funct. Mater.*, 2012, **22**, 1502–1510.
21 L. M. Cox, A. K. Blevins, J. A. Drisko, Y. Qi, Y. Ding, C. I. Fiedler-Higgins, R. Long, C. N. Bowman and J. P. Killgore, *Adv. Eng. Mater.*, 2019, **21**, 1900578.
22 J.-M. Restrepo-Flórez and M. Maldovan, *J. Membr. Sci.*, 2018, **566**, 301–306.
23 A. K. Blevins, L. M. Cox, L. Hu, J. A. Drisko, H. Lin, C. N. Bowman, J. P. Killgore and Y. Ding, *Macromolecules*, 2021, **54**, 44–52.
24 C. I. Fiedler-Higgins, L. M. Cox, F. W. DelRio and J. P. Killgore, *Small Methods*, 2019, **3**, 1800275.
25 A. C. Uzcategui, A. Muralidharan, V. L. Ferguson, S. J. Bryant and R. R. McLeod, *Adv. Eng. Mater.*, 2018, **20**, 1800876.
26 Z. V. Singh, L.-L. Tan, M. G. Cowan, Y.-W. Yang, W. Zhang, D. L. Gin and R. D. Noble, *J. Membr. Sci.*, 2017, **539**, 224–228.
27 L. Hu, J. Liu, L. Zhu, X. Hou, L. Huang, H. Lin and J. Cheng, *Sep. Purif. Technol.*, 2018, **205**, 58–65.
28 D. P. Nair, M. Podgórski, S. Chatani, T. Gong, W. Xi, C. R. Fenoli and C. N. Bowman, *Chem. Mater.*, 2014, **26**, 724–744.
29 D. Bodas and C. Khan-Malek, *Sens. Actuators B Chem.*, 2007, **123**, 368–373.
30 C. Lu, C. Wang, J. Yu, J. Wang and F. Chu, *ChemSusChem*, 2020, **13**, 893–902.
31 C. R. Szczepanski, C. S. Pfeifer and J. W. Stansbury, *Polymer*, 2012, **53**, 4694–4701.
32 Y. Liu, *J. Appl. Polym. Sci.*, 2013, **127**, 3279–3292.
33 H. S. Kim, S. I. Hong and S. J. Kim, *J. Mater. Process. Technol.*, 2001, **112**, 109–113.
34 O. Kolednik, J. Predan, F. D. Fischer and P. Fratzl, *Acta Mater.*, 2014, **68**, 279–294.
35 H. Lin and B. D. Freeman, *Macromolecules*, 2005, **38**, 8394–8407.
36 Y. Hirayama, Y. Kase, N. Tanihara, Y. Sumiyama, Y. Kusuki and K. Haraya, *J. Membr. Sci.*, 1999, 13.
37 G. K. Kline, J. R. Weidman, Q. Zhang and R. Guo, *J. Membr. Sci.*, 2017, **544**, 25–34.